iScience

CellPress
OPEN ACCESS

Article

Exploring host-commensal-pathogen dynamics in cell line and organotypic human intestinal epithelial models

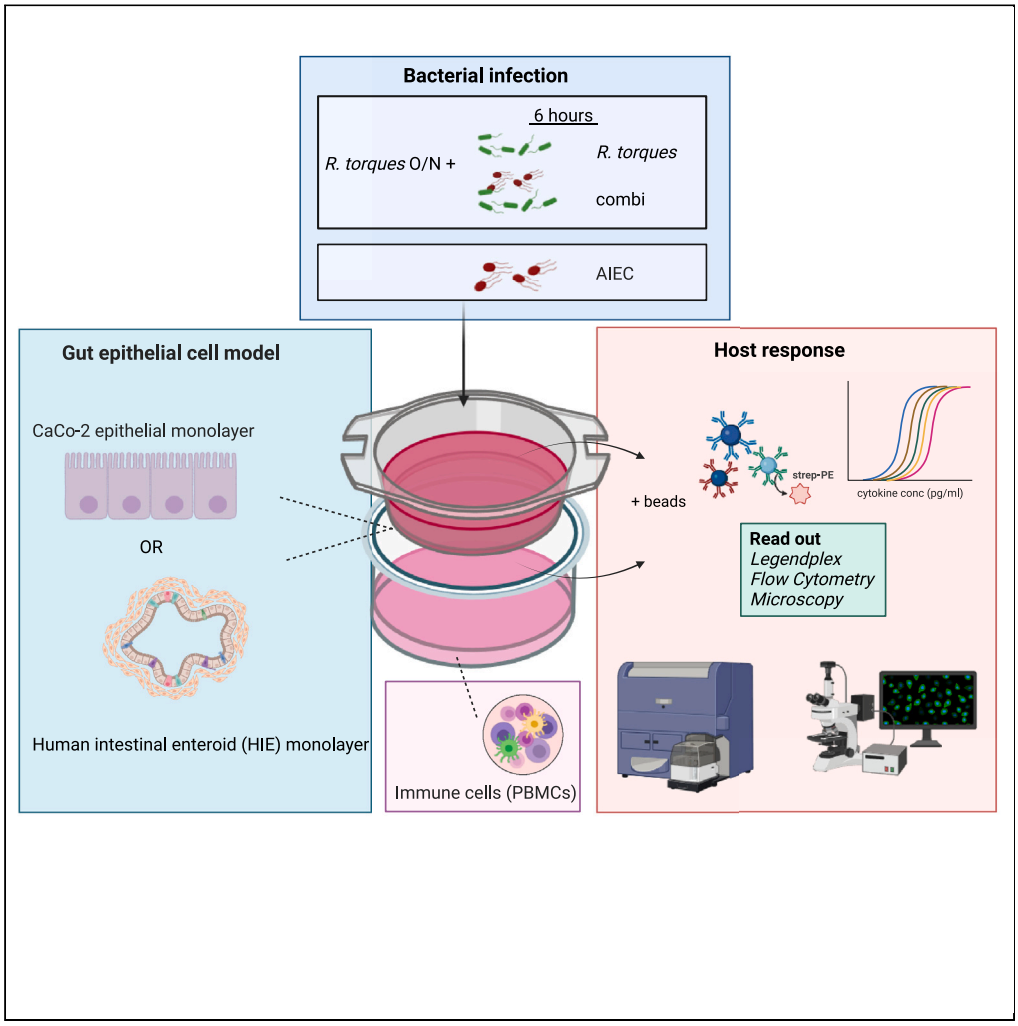

Nening M. Nanlohy, Nina Johannesson, Lucas Wijnands, ..., Katja C. Wolthers, Adithya Sridhar, Susana Fuentes

susana.fuentes@rivm.nl

Highlights

Our intestinal models are suitable to understand immune processes in the gut

These models are viable in co-culture with gut bacteria and in anaerobic conditions

R. torques and/or AIEC induced similar cytokine/chemokine profiles in both models

Co-culture with immune cells can trigger responses by the epithelium in both models

Nanlohy et al., iScience *27*, 109771
May 17, 2024
https://doi.org/10.1016/j.isci.2024.109771

iScience

CellPress
OPEN ACCESS

Article

Exploring host-commensal-pathogen dynamics in cell line and organotypic human intestinal epithelial models

Nening M. Nanlohy,[1,6] Nina Johannesson,[2,3,6] Lucas Wijnands,[1] Laura Arroyo,[1] Jelle de Wit,[1] Gerco den Hartog,[1,5] Katja C. Wolthers,[2] Adithya Sridhar,[2,3,4,7] and Susana Fuentes[1,7,8,*]

SUMMARY

Host and microbiome intricately interact in the ecosystem of the human digestive tract, playing a crucial role in our health. These interactions can initiate immune responses in the epithelial cells, which, in turn, activate downstream responses in other immune cells. Here, we used a CaCo-2 and a human intestinal enteroid (HIE) model to explore epithelial responses to both commensal and pathogenic bacteria, individually and combined. CaCo-2 cells were co-cultured with peripheral blood mononuclear cells, revealing downstream activation of immune cells. While both systems showed comparable cytokine profiles, they differed in their responses to the different bacteria, with the organoid system being more representative of responses observed in humans. We provide evidence of the pro-inflammatory responses associated with these bacteria. These models contribute to a deeper understanding of the interactions between the microbiota, intestinal epithelium, and immune cells in the gut, promoting advances in the field of host-microbe interactions.

INTRODUCTION

Interactions between commensal microbes, host epithelium, and the immune system in the gut mucosal environment contribute to maintenance of health.[1] This gut ecosystem plays an important role in the regulation of metabolic, endocrine, and immune functions, including the defense against infections.[2,3] Throughout life, the gut microbiota continuously evolves, influenced mainly by environmental and lifestyle factors.[4] Disturbances in the composition of the gut microbiota can impact the integrity of the gut barrier and are linked with the development of (chronic) inflammatory and metabolic diseases.[5–7] Furthermore, the proinflammatory state associated with aging, often referred to as inflammaging, has been associated with changes in the gut microbiome.[8–10] Recently, we showed that high abundance of the gut commensals *Ruminococcus torques* and *Escherichia coli*, often observed in inflammatory processes such as inflammatory bowel disease,[11–13] were associated with a pro-inflammatory immune profile in the aging population with influenza-like illness (ILI).[14] Such observational studies can provide new perspectives but are often confounded by a multitude of factors, especially in the aging population due to increased prevalence of comorbidities and medication use, and therefore, caution is warranted when making causal inferences.

To move beyond associations, more controlled mechanistic studies are key to obtain causal as well as deeper insights into the immunomodulatory effects of bacteria on the gut ecosystem. These should account for the trilateral interactions between human gut microbiota, epithelial intestinal cells, and immune cells in the gut microenvironment.[15,16] Currently, different *in vitro* models are available to study intestinal epithelial infections with varying levels of complexity and translatability.[17] Transwell co-cultures based on Caco-2 cell lines have been widely used to study intestinal host-microbe interactions.[18,19] The CaCo-2 monolayer, originated from a colon adenocarcinoma, can spontaneously differentiate to resemble a small intestine-like phenotype and thereby, mimics important properties of the intestinal epithelium.[18,20] These cultures can also be combined with peripheral blood mononuclear cells (PBMCs) to assess immune responses not only from the epithelial cells but also from immune cells mimicking the gut-associated lymphoid tissue. However, a gut epithelial model based on CaCo-2 cells lacks the degree of differentiation of epithelial cell subtypes present *in vivo*.[16] Recently developed human primary intestinal organoid models

[1]Center for Infectious Disease Control, National Institute for Public Health and the Environment, Bilthoven, the Netherlands
[2]OrganoVIR Labs, Department of Medical Microbiology, Amsterdam UMC, Location AMC, Amsterdam Institute for Infection and Immunity, University of Amsterdam, Amsterdam 1105 AZ, the Netherlands
[3]OrganoVIR Labs, Department of Pediatric Infectious Diseases, Emma Children's Hospital, Amsterdam UMC, Location AMC, University of Amsterdam, Amsterdam 1105 AZ, the Netherlands
[4]Emma Center for Personalized Medicine, Amsterdam UMC, Amsterdam, The Netherlands
[5]Laboratory of Medical Immunology, Radboudumc, Nijmegen, the Netherlands
[6]These authors contributed equally
[7]These authors contributed equally
[8]Lead contact
*Correspondence: susana.fuentes@rivm.nl
https://doi.org/10.1016/j.isci.2024.109771

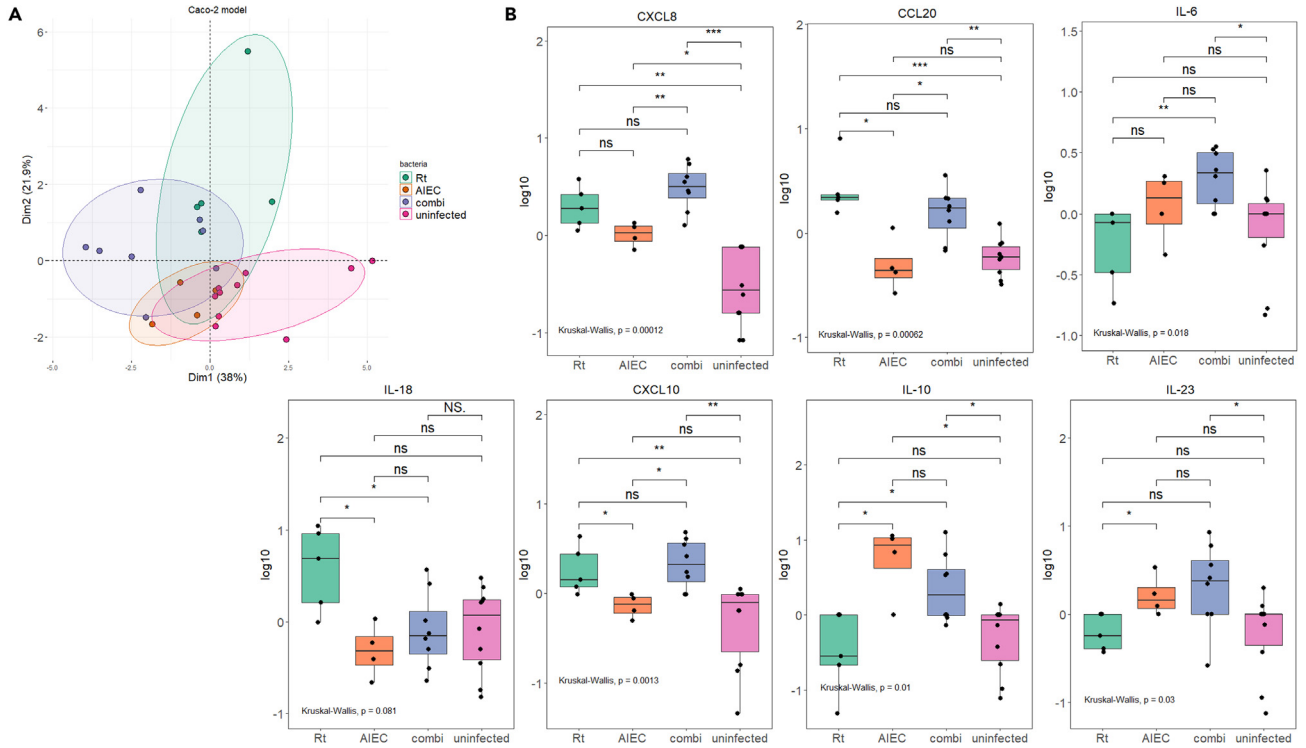

Figure 1. Cytokine profile of CaCo-2 cells stimulated with different bacteria individually and in combination

(A) Principal component analysis (PCA) of CaCo-2 cells stimulated with different bacteria individually and in combination. CaCo-2 cells were challenged with either *R. torques* and AIEC individually or in combination. PCA was based on the measured cytokines in the apical compartment. Rt =*Ruminococcus torques*. AIEC = adherent invasive *Escherichia coli*. Combi = combination of both bacteria. The first two principal axes explaine 59.9% of the variance (Dim = dimension). (B) Cytokine production of CaCo-2 cells stimulated with Rt, AIEC or combination. All data is represented as log10 normalized to the average per run for every cytokine or chemokine measured separately. Pairwise comparisons were done using the Wilcoxon test, group comparisons were performed with Kruskal Wallis test. ***p=<0.001 **p=<0.01 *p=<0.05 ns = p > 0.05 NS NS = p = 1.Rt =*Ruminococcus torques*. AIEC = adherent invasive *Escherichia coli*. Combi = combination of both bacteria. Assay was performed in triplicate, conditions were tested in at least 2 wells per experiment.

can alleviate some of these issues by recapitulating the *in vivo* cellular heterogeneity.[21–26] 2D intestinal epithelial monolayers, derived from primary human epithelial cells on Transwell inserts,[22,25] facilitate infection on the luminal side and enable studying complex multicellular responses as well as introducing biological variability. However, the high costs of these models are a drawback that limits experimental scale-up and breadth.[27]

In our study, we aimed to expand on our previous association study using these two aforementioned model systems to investigate interactions between key players in the gut ecosystem. We investigated the immune processes that occur in the gut epithelium primed with a commensal (*R. torques*) and subsequently challenged with a pathogenic (adherent invasive *E. coli*, AIEC) bacteria, selected for their previously observed synergistic interactions. We analyzed the individual and combined impact of these bacteria in the cytokine and chemokine response by both gut epithelial models and PBMCs. Our work shows a pro-inflammatory profile associated with these bacteria in the intestinal ecosystem.

RESULTS

Host response to *R. torques* and AIEC in a CaCo-2-based intestinal model

We assessed the innate immune response of the CaCo-2 epithelial monolayer to microbial exposure by determining the cytokine and chemokine profiles in the culture supernatants, after stimulation with *R. torques* overnight and, subsequently, challenged with either *R.torques* and AIEC individually or in combination for another 6 h (Figure S1). Principal component analysis (PCA) of the measured immune markers in the apical compartment showed clusters for the different bacterial stimulations (Figure 1A). Dimension (Dim) 1, explaining 38% of the variation, discriminated clusters of cells infected with the combination of both bacteria or uninfected, while Dim2 (21.9%) mostly separated the conditions stimulated with *R.torques (Rt)* from those stimulated with AIEC. Immune profiles measured differed significantly, except for those observed for stimulations with AIEC and the combination of AIEC and Rt (Figure 1B). The response of the CaCo-2 monolayer stimulated with Rt was dominated by the production of CXCL8, CXCL10, CCL20, and IL-18, while AIEC induced the production of IL-10, IL-6, and IL-23 (Figure 1B). When stimulated with the combination of bacteria, levels of cytokine production by individual bacteria were largely

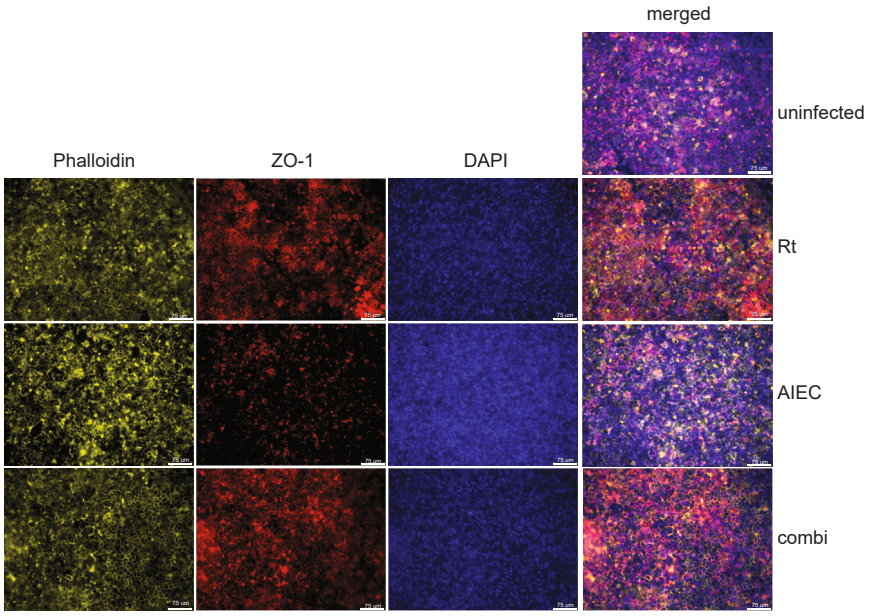

Figure 2. Effect of bacterial stimulation on the permeability of the CaCo-2 monolayer upon stimulation with Rt, AIEC or the combination

Representative images obtained by fluorescent microscopy of CaCo-2 cultures upon stimulation with the different bacteria, compared to the uninfected monolayer after 6 h. ZO-1 (tight junction, dsRed), Phalloidin (actin, cell skeleton, Y5), DAPI (nuclease, BLUE).

maintained, except for IL-18, which was significantly reduced when compared to Rt alone ($p = 0.03$, Figure 1B). Under all these conditions, no cytokine or chemokines were detected in the basolateral compartment.

To assess the integrity of the monolayer under these conditions, transepithelial electronical resistance (TEER) was measured throughout the experiment. The epithelial barrier was not disrupted by overnight stimulation with Rt or when Rt or AIEC were added for an additional 6 h. However, 24h stimulation with Rt or AIEC following the ON stimulation with Rt resulted in barrier loss (Figure S2). Immunofluorescent microscopy was carried out to validate the effect of bacterial stimulation on the tight junctions of the CaCo-2 monolayer. After the 6 h infection, cells were stained with ZO-1 (tight junction marker), DAPI (nuclease), and phalloidin (actin/cell cytoskeleton). Apical infection with *Rt* showed no impact on the organization of the tight junctions. Conversely, after stimulation with AIEC, the epithelial monolayer showed a partial loss of tight junctions and disorganization, which was less obvious when the infection was performed in combination with *Rt* (Figure 2).

Immune activation in co-culture with PBMCs after bacterial stimulation

To investigate how the presence of immune cells in the intestinal ecosystem modulates the epithelial response, PBMCs were included in the basolateral compartment of CaCo-2 cultures during the 6 h of infection. The cytokine profile of the CaCo-2 cells measured in the apical compartment, in the presence of PBMCs in the basolateral compartment, remained comparable to the previously observed responses (Figure 3A), with higher levels of CXCL8 and IL-6 (Figure 3B). This suggested that the cytokines detected in the apical compartment were mostly derived from the CaCo-2 cells. When co-cultured with PBMCs, the Rt-induced production of CCL20 was significantly inhibited by addition of AIEC to the overnight stimulation with Rt (Figure 3B). Although comparable cytokine profiles were observed in the apical compartment regardless of the presence or absence of basolateral PBMCs, PCA in co-cultures of CaCo-2 cells and PBMCs (Figure 3C) revealed distinctive profiles, primarily influenced by Dim2 (23.1%), potentially based on differences of the apical/basolateral polarization of the intestinal monolayer.

Closer examination of the different bacterial stimulations in the different compartments showed that responses in the apical compartment were largely uncorrelated with the specific stimulus, as no discernible clusters were observed (Figure 4). In general, CXCL8, IL-6, CCL2, and IL1-beta were mostly produced after stimulation with Rt, while IL-10, CXCL10, and IL12p70 were produced after AIEC stimulation and the combination of both bacteria. The responses in the basolateral compartment were, however, very distinct between the different bacterial stimulations (Figure 4). Production of IL-6, IL1-beta, and TNF-alpha was observed mainly after stimulation with AIEC and the combination of both bacteria. The responses to the commensal were very similar to the uninfected condition.

To investigate the activated fraction of the PBMCs, we performed immunophenotyping by flow cytometry of the basolateral compartment after the different conditions tested on the CaCo-2 model.

As expected, the percentages of the different cell subsets were similar in all conditions studied (Figure S3), stimulation with AIEC showed $CD4^+$ and $CD8^+$ T cells with a higher activated expression level ($CD4^+CD69^+$ and $CD8^+CD69^+$) when compared to stimulation with Rt alone. In addition, we used a transmigration assay to investigate which cell subsets were attracted by the chemokines produced by the CaCo-2 cells, using supernatants from the apical compartment in our gut model. Apical supernatants of all bacterial stimulations, particularly Rt, showed

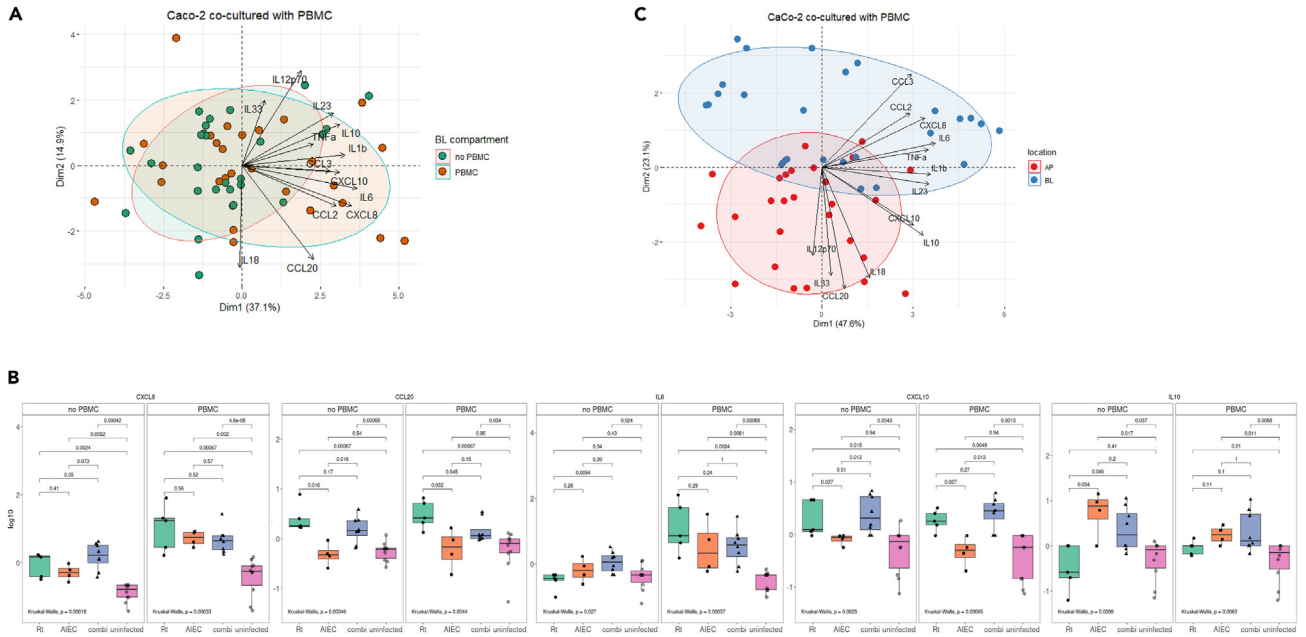

Figure 3. Cytokine profile of CaCo-2 cells co-cultured with PBMCs

(A) PCA of CaCo-2 cells co-cultured with and without PBMCs in the basolateral (BL) compartment. Cytokine profiles were measured in the apical (AP) compartment. Vectors display the contribution of distinct cytokines. The first two principal axes explained 52% of the variance (Dim = dimension).

(B) Cytokine production in the AP compartment of CaCo-2 cells co-cultured with or without PBMC included in the BL compartment. Pairwise comparisons were done using the Wilcoxon test, group comparisons were performed with Kruskal Wallis test. Rt = *Ruminococcus torques*. AIEC = adherent invasive *Escherichia coli*. Combi = combination of both bacteria.

(C) PCA of CaCo-2 cells co-cultured with PBMCs in the BL compartment. Cytokine profiles were measured in the apical (AP) and basolateral (BL) compartments. Vectors display the variables (cytokines measured) contributing to the first two dimensions (70,7%). Dim = dimension. This assay was performed in triplicate, conditions were tested in at least 2 wells per experiment.

migration of different cell subsets ($CD4^+$ and $CD8^+$ T cells, $CD19^+$ B cells, and monocytes) to the basolateral compartment with PBMCs (Figure S4).

Host response to *R. torques* and AIEC in a human intestinal enteroid monolayer model

Apical stimulation of the HIE monolayer with the different bacterial cultures resulted in similar responses compared to CaCo-2 cells. PCA of the measured immune markers revealed that both models showed not only an overlap in their cytokine and chemokine profiles (9 out of 11 cytokines, Figure 5A) but separation based on the pathogenicity of the bacteria can also be distinguished. While CaCo-2 cells stimulated with the commensal Rt produced significantly higher CCL20, CXCL10, and IL-18, we observed that CCL2 was higher in the HIE monolayer (Figure 5B). After stimulation with the pathogenic bacteria (AIEC with or without Rt), CaCo-2 cells produced significantly more IL-6 and IL-10 but less IL-18 when compared to the HIE monolayer. Independent of the model, stimulation with Rt showed higher production of CCL20, IL-6, IL-10, and CCL2 than stimulation with AIEC. In general, co-infection did not alter the cytokine production of each individual bacterium in the CaCo-2 model. However, in the HIE model, co-infection led to an increase in CCL20 and a decrease in CCL2 (Figure S5), potentially due to the diversity of cell types present in this model. In addition, despite the use of different donors within the HIE model, clusters based on the pathogenicity are still observed and likely contribute to the larger variation in the detected immune markers (Figures 5B and 5C).

Immunofluorescent microscopy of the enteroid monolayer showed that this was partially affected by stimulation with Rt alone, showing gaps in the monolayer (Figure 6A). However, stimulation with AIEC alone showed clear disruption of the monolayer and lysis of cells (Figure 6B). In this model in contrast with the CaCo-2 cell based, the monolayer was altered when incubated with Rt overnight but not as pronounced when compared to the stimulation by AIEC (Figure 6C).

Supernatants from the apical compartment in the human intestinal enteroid model were pooled and used in a transmigration assay to verify which cell subsets were attracted by the chemokines produced. As observed in the CaCo-2 cell-based model, apical supernatants of all bacterial stimulations showed migration of different cell subsets ($CD4^+$ and $CD8^+$ T cells, $CD19^+$ B cells, and monocytes) to the basolateral compartment with PBMCs (n = 3). In this model, no significant differences were observed between the commensal and pathogenic stimulations (Figure S6).

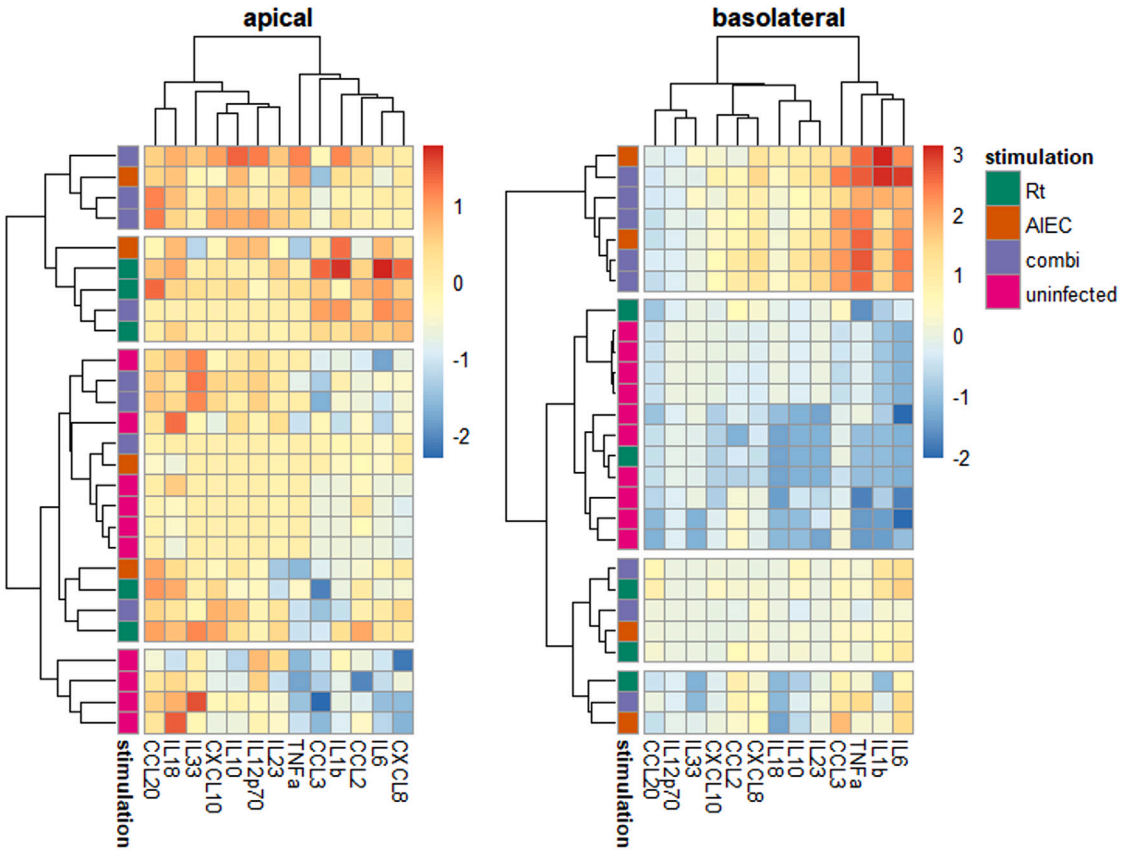

Figure 4. Heatmap of CaCo-2 cells co-cultured with PBMCs

Distribution of the different cytokines in the apical (AP) and basolateral (BL) compartments, measured over the different stimulations of the CaCo-2 cells co-cultured with PBMCs in the basolateral compartment. Rt =*Ruminococcus torques*. AIEC = adherent invasive *Escherichia coli*. Combi = combination of both bacteria. This assay was performed in triplicate, conditions were tested in at least 2 wells per experiment.

DISCUSSION

The complex interplay between microbes, the host epithelium and immune cells has only partly been elucidated.[5,6] In our study, we aimed to investigate the immune processes that occur in the gut epithelium using both a traditional CaCo-2 cell-based epithelial model and a more representative human intestinal enteroid model. Based on previous observations of a positive association between pro-inflammatory profiles and the presence of *E. coli* and *R. torques* in the gut ecosystem of individuals during an influenza-like illness (ILI),[14] we investigated how these bacteria modulated intestinal epithelial cell responses. Challenging of the epithelial monolayers with the commensal (*R. torques*) and pathogenic (adherent invasive *E. coli*, AIEC) bacteria revealed that we can investigate the pathogenicity of these bacteria, with an overlap in cytokine and chemokine profiles between the models. The bacteria induced different cytokine responses by the epithelial monolayers, and a higher cytopathology was observed for AIEC. Addition of PBMCs in the basolateral compartment of the CaCo-2 system during infection showed that the epithelial responses in the apical compartment are not modulated.

Several studies have shown that members of the *Ruminococcus* genus are associated not only with local inflammation-mediated disorders, such as IBD,[28,29] but also with inflammatory disorders at distant sites.[30,31] *R. torques* belongs to a group of commensals known to be associated with chronic gut inflammation.[28] In this study, we demonstrated that stimulation with *R. torques* alone induced pro-inflammatory responses by the epithelial cells, dominated by the production of CXCL8, CXCL10, CCL3, and IL-18. This proinflammatory profile was also observed during influenza-like illness, as shown by our previous study.[14] Also, these Rt-induced pro-inflammatory chemokines are involved in leukocyte and monocyte recruitment, which was corroborated by the transmigration assay with PBMCs. The innate immune system, as a first line in host defense, plays an important role in orchestrating downstream immune responses to pathogens, that could contribute to inflammation and ILI-like complaints.[32,33] In addition, exacerbated immune responses, besides direct epithelial damage by microorganisms, can also damage the epithelial barrier.[3]

The AIEC strain LF82, a strain generally associated with IBD and a plausible driver of intestinal inflammation,[11–13] has the capacity to adhere and invade the gut epithelial monolayer. AIEC can trigger signal transduction pathways, which could result in suboptimal epithelial control of invading pathogens.[12,13,34] In our study, stimulation of the epithelial monolayers with AIEC showed a distinct cytokine profile that differed from that of *R. torques*. While in the CaCo-2 model, the profile induced by AIEC was mainly driven by IL-10, IL-6, and IL-23 production, in

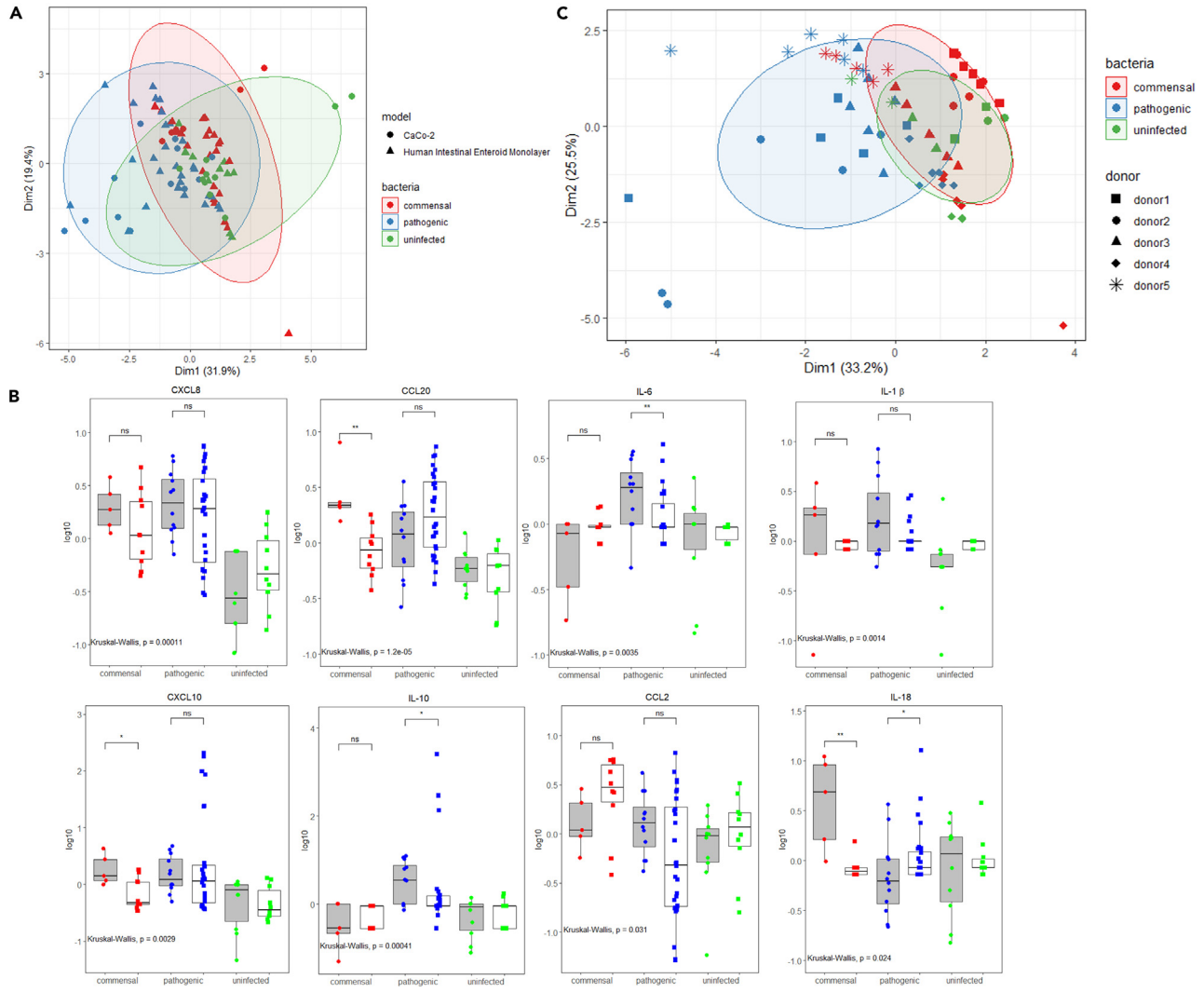

Figure 5. Cytokine profile of CaCo-2 monolayer vs. human intestinal enteroid monolayer

(A) PCA of CaCo-2 monolayer vs. human intestinal enteroid monolayer based on model and pathogenicity of the bacteria. Cytokine profiles were measured in the AP compartment in both models after stimulation with the different bacteria. Commensal = Rt, pathogenic = AIEC (individually or in combination with Rt).

(B) Cytokine production in apical (AP) compartment in both gut epithelial models. All data are represented as log10 normalized to the average per run for every cytokine or chemokine measured separately. Pairwise comparisons between the CaCo-2 model (gray box, circles) and HIE model (white box, squares) were done using the Kruskal-Wallis test. ***p=<0.001 **p=<0.01 *p=<0.05 ns = p > 0.05 NS NS = p = 1. Commensal = Rt, pathogenic = AIEC (individually or in combination with Rt).

(C) PCA of the cytokines measured in the apical compartment of a human intestinal enteroid monolayer stimulated with different bacteria. HIE monolayers of 5 different donors (represented with symbols) were challenged with either *R. torques* and AIEC individually or in combination. Different conditions were tested in duplicate wells. Commensal = Rt, pathogenic = AIEC (individually or in combination with Rt). Dim = dimension.

the HIE model, CXCL10 and CCL20 were also produced. Co-infection did not impact the cytokine production induced by the commensal, although IL-18 was significantly reduced by AIEC, suggesting an active inhibition of at least this particular component of the immune response. This suppressed response could be a result of a damaged epithelium followed by infection, leading to inflammation and potential barrier loss with the result of direct exposure of bacteria to immune cells. Local inflammasome-mediated IL-18 plays an important role in the regulation of homeostasis in the gut[35–39] and is induced upon infection with influenza virus with a role in the antiviral activity of the immune system.

We further investigated how *R. torques* and AIEC may impact downstream host immune responses in the gut epithelium. Addition of PBMCs to the basolateral compartment did not impact the cytokine and chemokine production of the CaCo-2 cells at the apical side. In fact, cytokine responses upon stimulation with Rt resemble the uninfected epithelium, suggesting a homeostatic response where PBMCs do not trigger additional responses in the CaCo-2 cells to the bacterial stimulations. On the basolateral compartment, while infection did

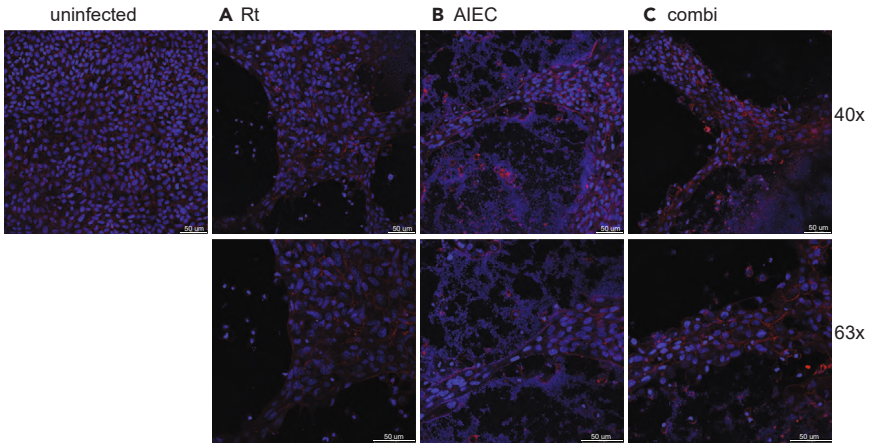

Figure 6. Effect of bacterial stimulation on the permeability of the HIE monolayer upon stimulation with Rt, AIEC or the combination

Representative images obtained by fluorescent microscopy (with 40× or 63× objective) of HIE cultures upon stimulation with the different bacteria, compared to the uninfected monolayer.

(A) Rt =*Ruminococcus torques*.

(B) AIEC = adherent invasive *Escherichia coli*.

(C) Combi = combination of both bacteria. Blue = Hoechst (nuclei marker), red = Epcam (epithelial cell marker).

not lead to production of immune markers in the absence of PBMCs, addition of these cells showed a proinflammatory cytokine profile mainly induced by infection with AIEC.

Despite the fact that the CaCo-2 cell-based epithelial model has been shown in ours and other studies as a useful tool to model infection and host responses, it has limitations due to the lack of cellular diversity. Recently developed human primary intestinal organoid models can alleviate some of these issues. Although these models are costly and technically challenging,[25] they provide more insights into host-pathogen interactions comparable to the *in vivo* situation.[22,40,41] In our study, comparison of the immune responses induced by the different bacteria in both models showed similar cytokine and chemokine profiles. In fact, stimulation with commensal and pathogenic bacteria can be clearly differentiated independent of the model. Stimulation of HIE with the pathogenic bacteria showed not only low production of CCL2, a member of chemotactic cytokines that attract macrophages and also enhances pro-inflammatory responses[42,43] but also inhibition in co-infection. In line with this, we observed higher production of IL-6 and IL-10 induced by stimulation with the pathogenic bacteria in both gut epithelial models. In addition, it has been established that *R. torques* can degrade the mucus layer by colonizing the intestinal mucosa[28] and release of mucins and other substrates from the mucus layer and serve as a substrate beneficial for AIEC to overgrow in the gut.[44] The main drawback of our CaCo-2 model is the fact that Caco-2 cells do not produce significant amounts of mucins under normal growth conditions.[45] The human intestinal enteroid monolayer model, on the contrary, contains all cell types of the intestinal epithelium present *in vivo*, including the MUC2 expressing goblet cells.[22] Fluorescent imaging of the human intestinal enteroid monolayer supports the hypothesis that overnight priming of the monolayer with *R. torques* is beneficial for invasion of AIEC, as gaps in the monolayer become visible.

Taken together, we demonstrate that both CaCo-2 cell-based model and a human intestinal enteroid (HIE) model are suitable to understand the immune processes that occur in the gut epithelium in the presence of commensal and pathogenic bacteria, nevertheless, both models have their own limitations. While the CaCo-2 model represents a simple cell culture model, it lacks the complexity to study the mechanisms of interaction between the commensal and pathogenic bacteria. The human intestinal enteroid model represents the epithelial cell composition *in vivo* more accurately but lacks the dynamics of the intestinal mucosa. Although the human enteroid model should be further examined on host immune responses, this model could be a more promising system and valuable tool to the complexity of gut-host-microbiome interactions. Moreover, increasing the complexity of the microorganisms added could give more insights into the immunomodulatory effects of bacteria on the gut ecosystem.

Limitations of the study

(1) The CaCo-2 model represents a simple cell culture model that is independent of donor variability, but it lacks the complexity of the cell types present in the intestinal epithelium, which are key to study the mechanisms of interaction between the commensal and pathogenic bacteria with the host in the gut.

(2) The human intestinal enteroid model better represents the epithelial cell composition *in vivo* but lacks the dynamics of the complete intestinal mucosa.

(3) The complexity and diversity of the intestinal microbiome is higher than that used in this study. Therefore, an increment of the complexity of the microorganisms added to the models could give more insights into the immunomodulatory effects of bacteria on the gut ecosystem.

STAR★METHODS

Detailed methods are provided in the online version of this paper and include the following:

- KEY RESOURCES TABLE
- RESOURCE AVAILABILITY
  - Lead contact
  - Materials availability
  - Data and code availability
- EXPERIMENTAL MODEL AND STUDY PARTICIPANT DETAILS
  - Bacterial cultures
  - Caco-2 cell culture
  - Human intestinal enteroid monolayer culture
- METHOD DETAILS
  - Infection and co-culture with immune cells
  - Immune profiling by Legendplex and flow cytometry
  - Migration assay
  - Immunofluorescence imaging
- QUANTIFICATION AND STATISTICAL ANALYSIS

SUPPLEMENTAL INFORMATION

Supplemental information can be found online at https://doi.org/10.1016/j.isci.2024.109771.

ACKNOWLEDGMENTS

This work was supported by the Dutch Ministry of Health, Welfare and Sport and by the PPP Allowance (Focus-on-Virus) made available by Health Holland, Top Sector Life Sciences & Health, to the Amsterdam UMC, location Amsterdam Medical Center to stimulate public–private partnerships. The funders had no role in the design of the study, data analysis, writing of the manuscript, or in the decision to publish the results.

The HIS mouse facility (Amsterdam UMC, The Netherlands) is acknowledged for providing fetal tissues. The authors would like to thank Dr. Kees Weijer, Mrs. Esther Siteur-van Rijnstra, Mrs. Cynthia A van der Linden, and Dr. Arie Voordouw for facilitating the provision of the fetal material. Cellular Imaging core facility of the Amsterdam UMC, The Netherlands is acknowledged for the advanced light microscopy support.

AUTHOR CONTRIBUTIONS

Conceptualization, S.F., J.d.W., G.d.H., and A.S.; methodology,N.N., N.J., L.W., and L.A.; formal analysis, N.N.; investigation, N.N, N.J., L.A., and L.W.; writing – original draft, N.N. and S.F.; writing – review and editing, J.d.W., G.d.H., and A.S.; funding acquisition, K.W., A.S., and S.F.; resources, N.J., K.W., and A.S.; supervision, J. d.W., G.d.H., A.S., and S.F.

DECLARATION OF INTERESTS

The authors declare no competing interests.

Received: November 28, 2023
Revised: February 26, 2024
Accepted: April 15, 2024
Published: April 18, 2024

REFERENCES

1. Gasaly, N., Hermoso, M.A., and Gotteland, M. (2021). Butyrate and the Fine-Tuning of Colonic Homeostasis: Implication for Inflammatory Bowel Diseases. Int. J. Mol. Sci. *22*, 3061. https://doi.org/10.3390/ijms22063061.
2. Rath, E., and Haller, D. (2022). Intestinal epithelial cell metabolism at the interface of microbial dysbiosis and tissue injury. Mucosal Immunol. *15*, 595–604. https://doi.org/10.1038/s41385-022-00514-x.
3. Turner, J.R. (2009). Intestinal mucosal barrier function in health and disease. Nat. Rev. Immunol. *9*, 799–809. https://doi.org/10.1038/nri2653.
4. Santoro, A., Bientinesi, E., and Monti, D. (2021). Immunosenescence and inflammaging in the aging process: age-related diseases or longevity? Ageing Res. Rev. *71*, 101422. https://doi.org/10.1016/j.arr.2021.101422.
5. Daniel, N., Lécuyer, E., and Chassaing, B. (2021). Host/microbiota interactions in health and diseases-Time for mucosal microbiology! Mucosal Immunol. *14*, 1006–1016. https://doi.org/10.1038/s41385-021-00383-w.
6. Cani, P.D., Bibiloni, R., Knauf, C., Waget, A., Neyrinck, A.M., Delzenne, N.M., and Burcelin, R. (2008). Changes in gut microbiota control metabolic endotoxemia-induced inflammation in high-fat diet-induced obesity and diabetes in mice. Diabetes *57*, 1470–1481. https://doi.org/10.2337/db07-1403.
7. Sugihara, K., and Kamada, N. (2021). Diet–Microbiota Interactions in Inflammatory Bowel Disease. Nutrients *13*, 1533.
8. Conway, J., and A Duggal, N. (2021). Ageing of the gut microbiome: Potential influences on immune senescence and inflammageing.

Ageing Res. Rev. *68*, 101323. https://doi.org/10.1016/j.arr.2021.101323.
9. Dowdell, A.S., and Colgan, S.P. (2021). Metabolic Host-Microbiota Interactions in Autophagy and the Pathogenesis of Inflammatory Bowel Disease (IBD). Pharmaceuticals *14*, 708. https://doi.org/10.3390/ph14080708.
10. Ragonnaud, E., and Biragyn, A. (2021). Gut microbiota as the key controllers of "healthy" aging of elderly people. Immun. Ageing *18*, 2. https://doi.org/10.1186/s12979-020-00213-w.
11. Martinez-Medina, M., Aldeguer, X., Lopez-Siles, M., González-Huix, F., López-Oliu, C., Dahbi, G., Blanco, J.E., Blanco, J., Garcia-Gil, L.J., and Darfeuille-Michaud, A. (2009). Molecular diversity of Escherichia coli in the human gut: new ecological evidence supporting the role of adherent-invasive E. coli (AIEC) in Crohn's disease. Inflamm. Bowel Dis. *15*, 872–882. https://doi.org/10.1002/ibd.20860.
12. Darfeuille-Michaud, A., Boudeau, J., Bulois, P., Neut, C., Glasser, A.L., Barnich, N., Bringer, M.A., Swidsinski, A., Beaugerie, L., and Colombel, J.F. (2004). High prevalence of adherent-invasive Escherichia coli associated with ileal mucosa in Crohn's disease. Gastroenterology *127*, 412–421. https://doi.org/10.1053/j.gastro.2004.04.061.
13. Jensen, S.R., Mirsepasi-Lauridsen, H.C., Thysen, A.H., Brynskov, J., Krogfelt, K.A., Petersen, A.M., Pedersen, A.E., and Brix, S. (2015). Distinct inflammatory and cytopathic characteristics of Escherichia coli isolates from inflammatory bowel disease patients. Int. J. Med. Microbiol. *305*, 925–936. https://doi.org/10.1016/j.ijmm.2015.10.002.
14. Fuentes, S., den Hartog, G., Nanlohy, N.M., Wijnands, L., Ferreira, J.A., Nicolaie, M.A., Pennings, J.L.A., Jacobi, R., de Wit, J., van Beek, J., and van Baarle, D. (2021). Associations of faecal microbiota with influenza-like illness in participants aged 60 years or older: an observational study. Lancet. Healthy Longev. *2*, e13–e23. https://doi.org/10.1016/S2666-7568(20)30034-9.
15. Venema, K., and van den Abbeele, P. (2013). Experimental models of the gut microbiome. Best Pract. Res. Clin. Gastroenterol. *27*, 115–126. https://doi.org/10.1016/j.bpg.2013.03.002.
16. von Martels, J.Z.H., Sadaghian Sadabad, M., Bourgonje, A.R., Blokzijl, T., Dijkstra, G., Faber, K.N., and Harmsen, H.J.M. (2017). The role of gut microbiota in health and disease: In vitro modeling of host-microbe interactions at the aerobe-anaerobe interphase of the human gut. Anaerobe *44*, 3–12. https://doi.org/10.1016/j.anaerobe.2017.01.001.
17. Qi, Y., Yu, L., Tian, F., Zhao, J., and Zhai, Q. (2023). In vitro models to study human gut-microbiota interactions: Applications, advances, and limitations. Microbiol. Res. *270*, 127336. https://doi.org/10.1016/j.micres.2023.127336.
18. Parlesak, A., Haller, D., Brinz, S., Baeuerlein, A., and Bode, C. (2004). Modulation of cytokine release by differentiated CACO-2 cells in a compartmentalized coculture model with mononuclear leucocytes and nonpathogenic bacteria. Scand. J. Immunol. *60*, 477–485. https://doi.org/10.1111/j.0300-9475.2004.01495.x.
19. Hoffmann, P., Burmester, M., Langeheine, M., Brehm, R., Empl, M.T., Seeger, B., and Breves, G. (2021). Caco-2/HT29-MTX co-cultured cells as a model for studying physiological properties and toxin-induced effects on intestinal cells. PLoS One *16*, e0257824. https://doi.org/10.1371/journal.pone.0257824.
20. Pearce, S.C., Coia, H.G., Karl, J.P., Pantoja-Feliciano, I.G., Zachos, N.C., and Racicot, K. (2018). Intestinal *in vitro* and ex vivo Models to Study Host-Microbiome Interactions and Acute Stressors. Front. Physiol. *9*, 1584. https://doi.org/10.3389/fphys.2018.01584.
21. Sato, T., and Clevers, H. (2013). Growing Self-Organizing Mini-Guts from a Single Intestinal Stem Cell: Mechanism and Applications. Science *340*, 1190–1194. https://doi.org/10.1126/science.1234852.
22. Roodsant, T., Navis, M., Aknouch, I., Renes, I.B., van Elburg, R.M., Pajkrt, D., Wolthers, K.C., Schultsz, C., van der Ark, K.C.H., Sridhar, A., and Muncan, V. (2020). A Human 2D Primary Organoid-Derived Epithelial Monolayer Model to Study Host-Pathogen Interaction in the Small Intestine. Front. Cell. Infect. Microbiol. *10*, 272. https://doi.org/10.3389/fcimb.2020.00272.
23. Rauth, S., Karmakar, S., Batra, S.K., and Ponnusamy, M.P. (2021). Recent advances in organoid development and applications in disease modeling. Biochim. Biophys. Acta Rev. Canc *1875*, 188527. https://doi.org/10.1016/j.bbcan.2021.188527.
24. Aknouch, I., Sridhar, A., Freeze, E., Giugliano, F.P., van Keulen, B.J., Romijn, M., Calitz, C., García-Rodríguez, I., Mulder, L., Wildenberg, M.E., et al. (2022). Human milk inhibits some enveloped virus infections, including SARS-CoV-2, in an intestinal model. Life Sci. Alliance *5*, e202201432. https://doi.org/10.26508/lsa.202201432.
25. García-Rodríguez, I., Sridhar, A., Pajkrt, D., and Wolthers, K.C. (2020). Put Some Guts into It: Intestinal Organoid Models to Study Viral Infection. Viruses *12*, 1288.
26. García-Rodríguez, I., van Eijk, H., Koen, G., Pajkrt, D., Sridhar, A., and Wolthers, K.C. (2021). Parechovirus A Infection of the Intestinal Epithelium: Differences Between Genotypes A1 and A3. Front. Cell. Infect. Microbiol. *11*, 740662. https://doi.org/10.3389/fcimb.2021.740662.
27. Puschhof, J., Pleguezuelos-Manzano, C., Martinez-Silgado, A., Akkerman, N., Saftien, A., Boot, C., de Waal, A., Beumer, J., Dutta, D., Heo, I., and Clevers, H. (2021). Intestinal organoid cocultures with microbes. Nat. Protoc. *16*, 4633–4649. https://doi.org/10.1038/s41596-021-00589-z.
28. Png, C.W., Lindén, S.K., Gilshenan, K.S., Zoetendal, E.G., McSweeney, C.S., Sly, L.I., McGuckin, M.A., and Florin, T.H.J. (2010). Mucolytic bacteria with increased prevalence in IBD mucosa augment *in vitro* utilization of mucin by other bacteria. Am. J. Gastroenterol. *105*, 2420–2428. https://doi.org/10.1038/ajg.2010.281.
29. Vereecke, L., and Elewaut, D. (2017). Spondyloarthropathies: Ruminococcus on the horizon in arthritic disease. Nat. Rev. Rheumatol. *13*, 574–576. https://doi.org/10.1038/nrrheum.2017.130.
30. Breban, M., Tap, J., Leboime, A., Said-Nahal, R., Langella, P., Chiocchia, G., Furet, J.P., and Sokol, H. (2017). Faecal microbiota study reveals specific dysbiosis in spondyloarthritis. Ann. Rheum. Dis. *76*, 1614–1622. https://doi.org/10.1136/annrheumdis-2016-211064.
31. Chua, H.H., Chou, H.C., Tung, Y.L., Chiang, B.L., Liao, C.C., Liu, H.H., and Ni, Y.H. (2018). Intestinal Dysbiosis Featuring Abundance of Ruminococcus gnavus Associates With Allergic Diseases in Infants. Gastroenterology *154*, 154–167. https://doi.org/10.1053/j.gastro.2017.09.006.
32. Wallace, K.L., Zheng, L.B., Kanazawa, Y., and Shih, D.Q. (2014). Immunopathology of inflammatory bowel disease. World J. Gastroenterol. *20*, 6–21. https://doi.org/10.3748/wjg.v20.i1.6.
33. Thaiss, C.A., Zmora, N., Levy, M., and Elinav, E. (2016). The microbiome and innate immunity. Nature *535*, 65–74. https://doi.org/10.1038/nature18847.
34. Barnich, N., Carvalho, F.A., Glasser, A.-L., Darcha, C., Jantscheff, P., Allez, M., Peeters, H., Bommelaer, G., Desreumaux, P., Colombel, J.-F., and Darfeuille-Michaud, A. (2007). CEACAM6 acts as a receptor for adherent-invasive E. coli, supporting ileal mucosa colonization in Crohn disease. J. Clin. Invest. *117*, 1566–1574. https://doi.org/10.1172/JCI30504.
35. Watanabe, D., Guo, Y., and Kamada, N. (2021). Interaction between the inflammasome and commensal microorganisms in gastrointestinal health and disease. EMBO Mol. Med. *13*, e13452. https://doi.org/10.15252/emmm.202013452.
36. Ratsimandresey, R.A., Indramohan, M., Dorfleutner, A., and Stehlik, C. (2017). The AIM2 inflammasome is a central regulator of intestinal homeostasis through the IL-18/IL-22/STAT3 pathway. Cell. Mol. Immunol. *14*, 127–142. https://doi.org/10.1038/cmi.2016.35.
37. Aguilera, M., Darby, T., and Melgar, S. (2014). The complex role of inflammasomes in the pathogenesis of Inflammatory Bowel Diseases - lessons learned from experimental models. Cytokine Growth Factor Rev. *25*, 715–730. https://doi.org/10.1016/j.cytogfr.2014.04.003.
38. Elinav, E., Strowig, T., Kau, A.L., Henao-Mejia, J., Thaiss, C.A., Booth, C.J., Peaper, D.R., Bertin, J., Eisenbarth, S.C., Gordon, J.I., and Flavell, R.A. (2011). NLRP6 inflammasome regulates colonic microbial ecology and risk for colitis. Cell *145*, 745–757. https://doi.org/10.1016/j.cell.2011.04.022.
39. Van Immerseel, F., Ducatelle, R., De Vos, M., Boon, N., Van De Wiele, T., Verbeke, K., Rutgeerts, P., Sas, B., Louis, P., and Flint, H.J. (2010). Butyric acid-producing anaerobic bacteria as a novel probiotic treatment approach for inflammatory bowel disease. J. Med. Microbiol. *59*, 141–143. https://doi.org/10.1099/jmm.0.017541-0.
40. Sato, T., Vries, R.G., Snippert, H.J., van de Wetering, M., Barker, N., Stange, D.E., van Es, J.H., Abo, A., Kujala, P., Peters, P.J., and Clevers, H. (2009). Single Lgr5 stem cells build crypt-villus structures *in vitro* without a mesenchymal niche. Nature *459*, 262–265. https://doi.org/10.1038/nature07935.
41. Nakamura, T. (2019). Recent progress in organoid culture to model intestinal epithelial barrier functions. Int. Immunol. *31*, 13–21. https://doi.org/10.1093/intimm/dxy065.
42. Reinecker, H.C., Loh, E.Y., Ringler, D.J., Mehta, A., Rombeau, J.L., and MacDermott, R.P. (1995). Monocyte-chemoattractant protein 1 gene expression in intestinal epithelial cells and inflammatory bowel disease mucosa. Gastroenterology *108*, 40–50. https://doi.org/10.1016/0016-5085(95)90006-3.
43. Gschwandtner, M., Derler, R., and Midwood, K.S. (2019). More Than Just Attractive: How

CCL2 Influences Myeloid Cell Behavior Beyond Chemotaxis. Front. Immunol. *10*, 2759. https://doi.org/10.3389/fimmu.2019.02759.

44. Huang, Y.L., Chassard, C., Hausmann, M., von Itzstein, M., and Hennet, T. (2015). Sialic acid catabolism drives intestinal inflammation and microbial dysbiosis in mice. Nat. Commun. *6*, 8141. https://doi.org/10.1038/ncomms9141.
45. Pan, F., Han, L., Zhang, Y., Yu, Y., and Liu, J. (2015). Optimization of Caco-2 and HT29 co-culture *in vitro* cell models for permeability studies. Int. J. Food Sci. Nutr. *66*, 680–685. https://doi.org/10.3109/09637486.2015.1077792.
46. Oliveira, M., Wijnands, L., Abadias, M., Aarts, H., and Franz, E. (2011). Pathogenic potential of Salmonella Typhimurium DT104 following sequential passage through soil, packaged fresh-cut lettuce and a model gastrointestinal tract. Int. J. Food Microbiol. *148*, 149–155. https://doi.org/10.1016/j.ijfoodmicro.2011.05.013.
47. Pinto, M.M.M. (1983). Enterocyte-like differentiation and polarization of the human colon carcinoma cell line Caco-2 in culture. Biol. Cell. *47*, 323–330.
48. Team, R. (2006). A language and environment for statistical computing. Computing *1*. https://doi.org/10.1890/0012-9658(2002)083[3097:CFHIWS]2.0.CO;2.
49. Ginestet, C. (2011). ggplot2: Elegant Graphics for Data Analysis. J. Roy. Stat. Soc. Stat. Soc. *174*, 245–246. https://doi.org/10.1111/j.1467-985X.2010.00676_9.x.
50. Lê, S., Josse, J., and Husson, F. (2008). FactoMineR: An R Package for Multivariate Analysis. J. Stat. Software *25*, 1–18. https://doi.org/10.18637/jss.v025.i01.
51. Kassambara, A., and Mundt, F. (2020). Extract and Visualize the Results of Multivariate Data Analyses. [R package factoextra version 1.0.7].
52. Oksanen, J., Simpson, G., Blanchet, F.G., Kindt, R., Legendre, P., Minchin, P., hara, R., Solymos, P., Stevens, H., Szöcs, E., et al. (2022). vegan community ecology package version 2.6-2 April 2022.

STAR★METHODS

KEY RESOURCES TABLE

REAGENT or RESOURCE	SOURCE	IDENTIFIER
Antibodies		
Human CD14 FITC	Biolegend	Cat#325604; RRID:AB_830676
Human CD8 PerCP-Cy5.5	Biolegend	Cat#301032; RRID:AB_893422
Human CD69 APC	Biolegend	Cat#310910; RRID:AB_314845
Human CD3 APC-R700	BD	Cat#659119; RRID:AB_2870468
BD Horizon Fixable Viability Stain780	BD	Cat#565388; RRID:AB_2869673
Human CD19 Pacific blue	Biolegend	Cat#302232; RRID:AB_2073118
Human CD16 BriliantViolet510	BD	Cat#563830; RRID:AB_2744296
HLA-DR BrilliatViolet650	BD	Cat#564231; RRID:AB_2738685
Human CD27 BrilliantViolet786	Biolegend	Cat#302832; RRID:AB_11219185
Human CD279(PD-1) PE	Biolegend	Cat#329906; RRID:AB_940483
Human CD56 PE/Dazzle594	Biolegend	Cat#318348; RRID:AB_2563563
Human CD38 PE-Cy7	eBioscience	Cat#25-0389-42; RRID:AB_1724057
Human CD45RO BrilliantUV395	BD	Cat#564291; RRID:AB_2744410
Human CD4 BrilliantUV737	BD	Cat#612748; RRID:AB_2870079
Phalloidin	Abcam	Cat#176759
Mouse anti-ZO-1	Invitrogen	Cat#33-9100; RRID:AB_87181
DAPI	Biolegend	Cat#422801
goat anti-mouse Alexa Fluor 555	Invitrogen	Cat#A32727; RRID:AB_2633276
polyclonal goat anti-human EpCAM	R&D Systems	Cat#AF960; RRID:AB_355745
Alexa Fluor 680 Donkey anti-goat	Thermo Fisher	Cat#A21084; RRID:AB_2535741
Hoechst 33342	Invitrogen	Cat#H3570
Bacterial and virus strains		
Ruminococcus torques (ATCC27756)	ATCC	ATCC27756
Escherichia coli (AIEC strain LF82)	provided by Prof. Dr. Peter Ernst (UCSD)	N/A
Biological samples		
Healthy blood bank donors	Sanquin (dutch blood bank)	N/A
Human foetal intestinal tissues (gestational age 14-19 weeks)	Private clinic in the Netherlands	N/A
Chemicals, peptides, and recombinant proteins		
Columbia agar with sheep blood	Oxoid	Cat#PB0123
Tryptone Bile X-Glucuronide (TBX)	Oxoid	Cat#CM0945
Gibco™ Dulbecco's modified Eagle's medium (DMEM) high glucose, HEPES	Thermo Fisher	Cat#42430
MEM Non-Essential Amino Acids Solution	Gibco	Cat#11140050
glutamin	Gibco	Cat#A2916801
gentamicin	Gibco	Cat#15750037
RPMI 1640 medium	Gibco	Cat#52400-0250
IntestiCult™ Organoid Growth Medium	Stemcell™ Technologies	Cat#06010
0.5 M EDTA	Invitrogen	Cat#15575-038
Pen-Strep	ThermoFisher	Cat#15140-122
Collagen type I	IBIDI	Cat#50201

(*Continued on next page*)

Continued

REAGENT or RESOURCE	SOURCE	IDENTIFIER
Matrigel	Corning	Cat#356231
Acetic acid	VWR	Cat#20103-295
PBS	Lonza	Cat#15140-122
TryplE™	Gibco	Cat#12605-010
Y-27632	Sigma	Cat#Y0503
IntestiCult™ OGM Human Basal Medium	Stemcell™ Technologies	Cat#100-0190
Advanced Dulbecco's Modified Eagle Medium/Nutrient Mixture F-12	Thermo Fisher	Cat#12634-028
HEPES	Sigma-Aldrich	Cat#H3375
Glutamax	Thermo Fisher	35050-038
FicollPaque		
Dimethyl sulfoxide (DMSO)	Sigma-Aldrich	Cat# D2650-5X5ML CAS: 67-68-5
Bovine serum albumin	Sigma-Aldrich	Cat#A4503
paraformaldehyde	VWR chemicals	Cat#97.135.000
Triton X-100	Merck	Cat#1.08603.1000
Methanol	VWR	Cat#20847.240
Sudan Black B	Sigma-Aldrich	Cat#199664-25G
Ethanol 96%	Fisher Scientific	Cat#13217993
SEA BLOCK Blocking buffer	Thermo Fisher	Cat#37527
Tris-buffered saline	EMD Millipore	Cat#524750
Tween20	Sigma-Aldrich	Cat#P1379-25ML
ProLong™ Glass Antifade Mountant	Thermo Fisher	Cat#P36984
Liquid Blocker Super PAP Pen	Daido sanyo Co.Japan	Cat#A-PAP Pen Regular
Critical commercial assays		
LEGENDplex™ custom-made Panel (13-plex)	Biolegend	Cat#92919
Experimental models: Cell lines		
CaCo-2 cells	ATCC	HTB-37
Software and algorithms		
R v4.2.0 and RStudio (v2022)		V4.2.0
FlowJo Software	BD	V10.6.2
Leica LAS X Software	Leica Microsystems	V3.4.2
LEGENDplex™ Data Analysis Software	Biolegend	https://www.biolegend.com/en-us/immunoassays/legendplex/support/software
Other		
FACS Fortessa X20	BD	
FACS CantoII	BD	
FACS Symphony	BD	
EVOM-2 voltohmmeter	World Precision Instruments	EVOM2
Anoxamat	Hettich instruments	
Leica Dmi8 inverted Fluorescence microscope with Leica DFC7000 GT camera	Leica Microsystems	
Leica TCS SP8-X microscope	Leica Microsystems	SP8-X

RESOURCE AVAILABILITY

Lead contact

Further information and requests should be directed to and will be fulfilled by the lead contact, Susana Fuentes (susana.fuentes@rivm.nl).

Materials availability

There are restrictions to the availability of fetal tissue and subsequent derivatives due to material transfer agreements between the Amsterdam UMC and a private clinic. This study did not generate new unique reagents.

Data and code availability

- Data: All data reported in this paper will be shared by the lead contact upon request.
- Code: This paper does not report original code.
- Any additional information required to reanalyze the data reported in this paper is available from the lead contact upon request.

EXPERIMENTAL MODEL AND STUDY PARTICIPANT DETAILS

Bacterial cultures

Bacterial cultures of *Ruminococcus torques* (ATCC27756) and an adherent/invasive Escherichia coli (AIEC strain LF82), and CaCo-2 cells were prepared as previously described.[14] For *in vitro* experiments, *R. torques* were cultured overnight at 37°C under anaerobic conditions (Anoxomat, Hettich Instruments) and AIEC at 37°C under aerobic conditions. Bacteria were inoculated on the apical (AP) side of the epithelial monolayer at approximately 10e9 CFU/mL. Enumeration of unbound bacteria was performed after plating 10-fold dilutions of the Triton-extracts (data not shown). Columbia agar with sheep blood was used for determining *R.torques* and *AIEC*. In addition, Tryptone Bile X-Glucuronide (TBX) plates were used for *AIEC*.

Caco-2 cell culture

Caco-2 cells were cultured and differentiated, essentially as described before.[46] In more detail, Caco-2 cells, obtained from the American Type Culture Collection (ATCC, HTB-37, Manassas, USA), were routinely kept in culture medium [Dulbecco's Modified Eagle's (DMEM, Gibco) supplemented with 10% heat-inactivated fetal bovine serum (Sigma-Aldrich), 1% non-essential amino acids (Gibco), 1% glutamine 100× (Gibco) and 0.1% gentamicin (50.0 mg/ml, Gibco)] in 75 cm2 flasks (Corning Incorporated, NY, USA). The cells were grown to confluence in 7 days, and passaged on to new 75 cm^2 flasks at a concentration of 1x106 cells/10 mL medium at 37°C in a humidified atmosphere of 95% air and 5% CO_2. Differentiation of the Caco-2 cells into cells simulating the small intestinal epithelium[47] was achieved by culturing the cells in monolayers on the apical side of Millicell® inserts (Millicell Hanging cell culture insert, PET 3.0 μm, 24-well, Millipore). For this, Caco-2 cells were seeded at a density of 1.6×10^5 cells/mL, and growth medium was changed every 2 or 3 days. These cells are known to be fully differentiated after being cultured for 14 days.

Human intestinal enteroid monolayer culture

Ethics statement

Human foetal intestinal tissues (gestational age 14-19 weeks) were obtained from the HIS Mouse Facility of the Amsterdam UMC through a private clinic. All material were collected from donors from whom a written informed consent for the use of the material for research purposes had been obtained by the clinic. These informed consents are kept together with the medical record of the donor by the clinic and information provided (age of the donor and gestational age of the foetus) to the Amsterdam UMC does not allow for identification of the donor without disproportionate efforts. The use of the foetal material and anonymized material for medical research purposes is covered by Dutch law (Wet foetaal weefsel and Article 467 of Behandelingsovereenkomst).

Isolation and culture of intestinal crypts

Intestinal crypts containing intestinal stem cells were isolated from whole human foetal small intestine. Briefly, foetal small intestine was cleaned by removing fat and mesothelium as much as possible. The tissue was cut open longitudinally and further cut into small 5x5 mm pieces. The tissue pieces were washed 15 to 20 times with cold PBS. Intestinal cells were then dissociated in a 2mM EDTA (Invitrogen, 15575-038) solution for 30 minutes at 4°C. Following incubation, the EDTA was inactivated using a 10% FCS (Sigma-Aldrich, F7524) in PBS (Lonza, 15140-122) solution and intestinal crypts were collected from the tissue pieces by washing and collecting the supernatant. The supernatant was passed through a 70μm cell strainer and intestinal crypts were cultured in 3x 10 μL Matrigel (Corning, 356231) domes per well in a 24-well plate. 500 μL of IntestiCult™ Organoid Growth Medium (Stemcell™ Technologies, 06010), supplemented with 100 U/mL Pen-Strep (ThermoFisher, 15140-122) to maintain enteroid cultures at 37°C, 5% CO2. Every 2-3 days medium was changed and enteroids were passaged twice a week by mechanical dissociation as described previously.[22]

Millicell® inserts (Millicell Hanging cell culture insert, PET 3.0 μm, 24-well, Millipore) were coated with 100 μL of 20 μg/mL collagen type I (5 mg/mL, rat tail, IBIDI, 50201) in 0.01% (v/v) acetic acid (VWR, 20103-295) for 1 h at room temperature. Collagen solution was aspirated and

inserts were washed twice with PBS (Lonza, 15140-122). Enteroids were then harvested on day 4 after passaging, by enzymatic dissociation using TryplE™ (Gibco, 12605-010) for 10 min at 37°C. Subsequently, 100 μL of a 1*10e6 cells/mL cell suspension was added to the AP side of the coated inserts and 600 μL of IntestiCult™ Organoid Growth Medium, supplemented with 10 μM Y-27632 (Sigma, Y0503), was added to the basolateral (BL) side. After 3 days, medium was changed and fresh medium without Y-27632 was added. After 7 days, medium was changed to differentiation medium containing a 1:1 mixture of IntestiCult™ OGM Human Basal Medium (#100-0190) and Advanced Dulbecco's Modified Eagle Medium/Nutrient Mixture F-12 (DMEM/F12, ThermoFisher Scientific, 12634-028) supplemented with 1% Pen-Strep, 1% HEPES (Sigma-Aldrich, H3375) and 1% Glutamax (ThermoFisher, 35050-038) to induce differentiation. Medium was refreshed again on day 10 and 13.The monolayers were cultured for 14 days after cell seeding, prior to infection,.

On days 3, 7, 10, and 14 Trans-epithelial electrical resistance (TEER) was measured (EVOM-2 voltohmmeter, World Precision Instruments) 10 min after medium change. Average TEER values were calculated from three measurements per insert. To calculate resistance to surface area (Ω*cm2) the background TEER (empty insert coated with collagen) was subtracted and the result was multiplied by the surface area of the insert (0.3 cm^2). As a quality control, only inserts with TEER values above 200 Ω*cm2 were used in infection experiments.

METHOD DETAILS

Infection and co-culture with immune cells

Epithelial monolayers were washed three times with sterile PBS, and the cells were placed in culture medium without antibiotics and FCS. Subsequently, monolayers were incubated with or without *R. torques* (approx. 10e9 CFU/mL) under anaerobic conditions at 37°C overnight. The next day, AIEC or *R. torques* (approx. 10e9 CFU/mL, multiplicity of infection of 10 (MOI10))) were added to the plate and incubated at 37°C for an additional 6h under anaerobic conditions. Supernatants were harvested for cytokine measurement. Optimal conditions for bacterial infection of the monolayers was assessed by measuring the kinetics of bacterial growth and determining cell viability by microscopy (data not shown).

To investigate the crosstalk between the gut epithelial cells and immune cells, PBMCs were incorporated in the CaCo-2 model. Peripheral blood mononuclear cells (PBMCs) from healthy blood-bank donors were isolated by Ficoll-Paque density centrifugation, cryopreserved and stored at -135°C in 10% dimethyl sulfoxide (DMSO, Sigma Aldrich) and foetal calf serum (FCS) until further use. After thawing, PBMCs (in RPMI/10%FCS without antibiotics, 10e6 cells/well) were added to the basolateral compartment of Transwell® inserts on which CaCo-2 cells were cultured apically. Bacterial infection was carried out as described above, and incubated with 5% O_2 at 37°C overnight.

Supernatants from both AP and BL compartments were harvested and stored at -20°C for further cytokine measurements, and PBMCs were analysed by flow cytometry.

Immune profiling by Legendplex and flow cytometry

Immune profiles in supernatants were measured following manufacturer's instructions with a multiplex bead-based assay, which includes the following cytokines and chemokines: CXCL8 (IL-8), IL-6, IL-10, IL1-beta, IL-18, TNF-alpha, CXCL10 (IP-10), CCL3 (MIP1-alpha), CCL20 (MIP3-alpha), CCL2 (MCP-1), IL-23, IL-33 and IL-12p70 (LEGENDplex™ custom-made Panel (13-plex), BioLegend, San Diego, CA, USA). In brief, standards or supernatants and assay buffer were added to the wells, together with mixed beads and detection antibodies. The plate was subsequently covered and incubated while shaking at 900 RPM for 2h at room temperature, after which Streptavidin-PE (SA-PE) was added to each well. After 30 min incubation, the plate was washed to remove unbound proteins. Subsequently, the samples were acquired by flow cytometry (FACS Canto II, BD, San Jose, CA, USA) and concentrations were calculated using the LEGENDplex™ Data Analysis Software (BioLegend).

After harvesting supernatants, PBMCs from the basolateral compartment were analysed for immunophenotyping (monocytes, T cells and activation and exhaustion markers) by flow cytometry. Briefly, cells were washed with 0.5% BSA/PBS (PBA) and incubated 15 min with a mixture of antibodies covering the different cell types (see Table S1). Samples were acquired on a FACS Symphony (BD) and analysed using FlowJo V10.6.2 Software.

Migration assay

Lymphocyte migration was determined by seeding 2x10e6 PBMCs in the AP chamber of a Corning HTS Transwell ® inserts 96-well permeable support with 3.0 μm pore polycarbonate membrane. Two hundred microliters of supernatant from the AP side of the gut epithelial model were added to the BL compartment of the Transwell ® inserts system and the plates were incubated for 2 h at 37°C and 5% CO_2. After incubation, cells from the BL compartment were collected and cell type and marker expression was determined with a LSRFortessa X-20 (BD). Data were analysed using FlowJo software V10.6.2 Software. Count beads were used to determine absolute number of cells.

Immunofluorescence imaging

Inserts with CaCo-2 cells were fixed in paraformaldehyde (4% v/v) for 15 min at 37°C. Cells were permeabilized with 0.1% (v/v) Triton X-100 for 5 min, blocked with 1% (v/v) BSA, 2% (v/v) Goat-serum (Biolegend) and 0.05% (v/v) Triton X-100 in PBS for 30 min. Subsequently, the cells were stained with Phalloidin (staining actin) and mouse anti-ZO-1 (10 μg/ml, Clone ZO1-1A12, staining tight junctions) for 1 h at 37°C. After washing, goat anti-mouse Alexa Fluor 555 (ZO-1 staining, Biolegend), as a secondary staining, was added for 1 h at 37°C. Nuclei were stained with DAPI (300 nM) for 10 min at 37°C. The polyester membrane containing the cells was excised from the Transwell® insert, placed on a microscopy

slide, and embedded in ProLong™ Diamond Antifade Mountant (Invitrogen). Images were captured with a Leica Dmi8 inverted Fluorescence microscope using a Leica DFC7000 GT camera and LAS X 3.4.2 software, with a 40× objective.

Enteroid monolayers were fixed in paraformaldehyde (4% v/v) for 15 min at 37°C and stored in PBS at 4°C. Ice-cold 100% methanol (VWR Chemicals, 20847.240) was added to the inserts for 5 min at room temperature to permeabilize the cells. Methanol was removed and 0.3% (w/v) Sudan Black B (Sigma-Aldrich, 199664-25G) in 70% Ethanol was added for 30 minutes at room temperature. Inserts were removed with a tweezer and washed by immersing the insert into PBS five times. Subsequently, blocking was performed overnight using SEA BLOCK Blocking buffer (ThermoFisher, 37527) at 4°C. Microscopy slides (VWR, 631-1161) were prepared by circling two parts of the slide with Liquid Blocker Super PAP Pen (Daido Sangyo). Using a scalpel, membranes were cut out from the inserts and placed on the slides within the PAP circle. This was followed by incubation of the cut membranes with primary antibody polyclonal goat anti-human EpCAM (R&D Systems, AF960, 1:100 in SEA BLOCK) overnight at 4°C in a humidified chamber. Membranes were then gently washed three times with Tris-buffered saline (TBS)-Tween (150 mM NaCl, 50 mM Tris-HCL buffer and 1% w/v Tween20) (TBS; EMD Millipore 524750, Tween20; Sigma-Aldrich) and incubated in Alexa Fluor 680 Donkey anti-goat secondary (ThermoFisher, A21084) (1:500 in SEA BLOCK) and Hoechst 33342 (Invitrogen, H3570, 1:1000 in SEA BLOCK) for 2 hours at RT. Membranes were gently washed three times with PBS and mounted using ProLong™ Glass Antifade Mountant (P36984, ThermoFisher Scientific). Slides were imaged using Leica TCS SP8-X microscope with HC Plan Apochromat 40× and 63× oil objective and analysed using Leica LAS X Software (Leica Microsystems).

QUANTIFICATION AND STATISTICAL ANALYSIS

All data analyses were performed in R v4.2.0[48] and RStudio (v2022) with packages ggplot2[49] and stats[48] among others. Before evaluation of the cytokine data, values were normalized into averages of the logarithms centered by the subtraction of the within-run averages to correct for potential batch effects. Principal component analysis (PCA) was performed using the built-in R function prcomp() and visualized with R packages FactoMineR[50] and factoextra.[51] Pairwise comparisons between the different conditions tested were done using permutational multivariate analysis of variance (PERMANOVA) with the adonis function of the vegan package[52] at 999 permutations.